Fluctuation dynamics of a single magnetic chain

Adriana S. Silva,[1] Robert Bond,[1] Franck Plouraboué,[2] and Denis Wirtz[1,*]
[1]*Department of Chemical Engineering, The Johns Hopkins University, 3400 North Charles Street, Baltimore, Maryland 21218*
[2]*Ecole Supérieure de Physique et Chimie Industrielle de la Ville de Paris, Laboratoire PMMH, 10 rue Vauquelin, F-75231 Paris Cedex, France*
(Received 27 March 1996)

''Tunable'' fluids such as magnetorheological (MR) and electrorheological (ER) fluids are comprised of paramagnetic or dielectric particles suspended in a low-viscosity liquid. Upon the application of a magnetic or electric field, these fluids display a dramatic, reversible, and rapid increase of the viscosity. This change in viscosity can, in fact, be tuned by varying the applied field, hence the name ''tunable fluids.'' This effect is due to longitudinal aggregation of the particles into chains in the direction of the applied field and the subsequent lateral aggregation into larger semisolid domains. A recent theoretical model by Halsey and Toor (HT) explains chain aggregation in dipolar fluids by a fluctuation-mediated long-range interaction between chains and predicts that this interaction will be equally efficient at all applied fields. This paper describes video-microscopy observations of long, isolated magnetic chains that test HT theory. The measurements show that, in contrast to the HT theory, chain aggregation occurs more efficiently at higher magnetic field strength (H_0) and that this efficiency scales as $H_0^{1/2}$. Our experiments also yield the steady-state and time-dependent fluctuation spectra $C(x,x')\equiv\langle[h(x)-h(x')]^2\rangle^{1/2}$ and $C(x,x',t,t')\equiv\langle[h(x,t)-h(x',t')]^2\rangle^{1/2}$ for the instantaneous deviation $h(x,t)$ from an axis parallel to the field direction to a point x on the chain. Results show that the steady-state fluctuation growth is similar to a biased random walk with respect to the interspacing $|x-x'|$ along the chain, $C(x,x')\approx|x-x'|^{\alpha}$, with a roughness exponent $\alpha=0.53\pm0.02$. This result is partially confirmed by Monte Carlo simulations. Time-dependent results also show that chain relaxation is slowed down with respect to classical Brownian diffusion due to the magnetic chain connectivity, $C(x,x',t,t')\approx|t-t'|^{\beta}$, with a growth exponent $\beta=0.35\pm0.05<\frac{1}{2}$. All data can be collapsed onto a single curve according to $C(x,x',t,t')\approx|x-x'|^{\alpha}\psi(|t-t'|/|x-x'|^{z})$, with a dynamic exponent $z=\alpha/\beta\cong1.42$.
[S1063-651X(96)13911-8]

PACS number(s): 47.50.+d, 83.80.Gv, 83.20.Jp

I. INTRODUCTION

Over the past decade, a great deal of attention has been focused on the development of a new class of fluids, termed ''tunable'' fluids [1,2]. Electrorheological (ER) and magnetorheological (MR) fluids belong to this class. These fluids offer the promise of fast-response devices, which would efficiently interface mechanical components with electronic controls. Advantages of such devices include fast switching speed, miniaturization, and continuously variable control. The inherent value of these materials lies in their ability to quickly and reversibly change from a liquidlike state to a semisolid state when subjected to an electric or magnetic field, with a response time on the order of a few milliseconds [3]. This rapid ''tunable'' phase transition induces a rapid and drastic increase of the fluid viscosity [4].

ER fluids are comprised of fine dielectric particles immersed in a medium of different dielectric constant (i.e., silicone oil, water) [3]. Due to particle chaining in the direction of the applied electric field, the fluid undergoes a change in viscosity [3,4]. The development of ER fluids dates back to the 1940s, with the original work by Winslow [5]. The system used was comprised of an ER fluid based on dispersed, moist silica gel. Winslow observed that, upon application of an electric field, particles suspended in oil formed fibrous structures aligned with the field. In addition, working with field strengths on the order of 3 kV/mm, he determined that the shear stress $[\tau(E)-\tau(0)]$ was dependent on the square of the applied voltage. Winslow postulated many applications of ER fluids and described their use in clutches, brakes, and valves [3].

After a brief period of intense interest, work in the field dwindled for almost 30 years. The next extensive work was carried out by Klass and Martinek [6,7], who reported their results from ER fluids comprised of silica and calcium titanate. In two landmark papers [6,7], these authors described the $\tau(E)-\gamma$ interdependence and how shear stress (τ) is effected by several variables such as electric field strength (E), frequency (f), fluid composition (φ), temperature (T), and shear rate ($\dot{\gamma}$). Klass and Martinek [7] also presented bulk conductance (σ) measurements of the fluid as a whole and the consequent power demand of these typical ER systems under use.

Our work focuses on the magnetic analogs of ER fluids, which are termed magnetorheological fluids (MR fluids). Similar to ER fluids in many respects, MR fluids exhibit several key differences, among which are the absence of charge, higher strength, better stability over broader temperature range, and less stringent manufacturing requirements [1]. In addition, MR fluids are experimentally easier to work with as several potential difficulties are avoided such as electrode polarization and direct contact with the fluid. MR fluids, therefore, constitute model ''tunable'' fluids with prop-

*Author to whom correspondence should be addressed.

erties similar to ER fluids but with reduced potential experimental artifacts. Moreover, MR fluids are not affected by chemical impurities normally encountered during manufacturing and the raw materials are nontoxic and environmentally safe. Despite these advantages, there is currently no large scale fabrication of mechanical devices using MR fluids as the tribological properties have yet to be well characterized [8].

Despite all the interest in ER fluids, surprisingly few studies have been performed on MR fluids. This is difficult to reconcile with the advantages that MR fluids present. MR fluids, as mentioned, are the true magnetic analogs of ER fluids. They are not ferrofluids or magnetic liquids, which are typically made of nanoparticles and used for applications such as hermetic sealing; instead, MR fluids are generally comprised of magnetizable submicrometer particles suspended in a liquid medium such as water or oil [1]. These paramagnetic particles (no permanent dipole) have recently found a wide range of applications such as separating agents for biopolymers and cells [9] and for the micromanipulation of individual biological macromolecules [10]. MR fluids display the viscosity of a concentrated colloidal suspension in the absence of a magnetic field; under a magnetic field, they exhibit shear-thinning characteristics and are usually defined in terms of a Bingham plastic model [4]. Halsey and Toor [11,12] proposed a comprehensive theory to model the lateral chain aggregation process for MR and ER fluids.

The present work develops a link between the microscopic structure of these fluids and their bulk properties. Previous works suggest that lateral chain aggregation into columns via attractive dipolar interaction is the principal cause of the enhanced viscosity effects [13–30]. Our goal is to help uncover the mechanism by which two chains far apart can interact. It is assumed that the combined effects of direct dipole-dipole interaction and thermal-fluctuation-mediated long-range magnetic interactions govern chain interactions and, therefore, the kinetics of chain aggregation. This work reports comprehensive video-microscopy experiments and preliminary numerical studies of single chain dynamics.

II. THEORETICAL BACKGROUND

A. Introduction

Upon the application of an external magnetic field strong enough to overcome the random thermal forces (or Brownian forces), the interaction between induced dipoles in each of the particles causes them to aggregate into chains. Chaining of paramagnetic particles via anisotropic dipole-dipole interactions is well understood: the dipole-dipole interaction potential between two particles [23],

$$U(r,\theta)=\frac{(\mu^2/4\pi\mu_0)(1-3\cos^2\theta)}{r^3} \tag{1}$$

promotes linear aggregation of neighboring Brownian particles in the field direction as long as the angle θ between the line joining their centers and the direction of the field is smaller than $\arccos(1/\sqrt{3})$. Here, $\mu=4\pi a^3\mu_0\chi H_0/3$ is the induced magnetic dipole moment of a particle. Under typical experimental conditions, this linear particle aggregation takes place extremely rapidly (less than 1 s). This competition between the thermal forces and the dipole-dipole forces can be characterized by a single dimensionless parameter, λ, given by [23]

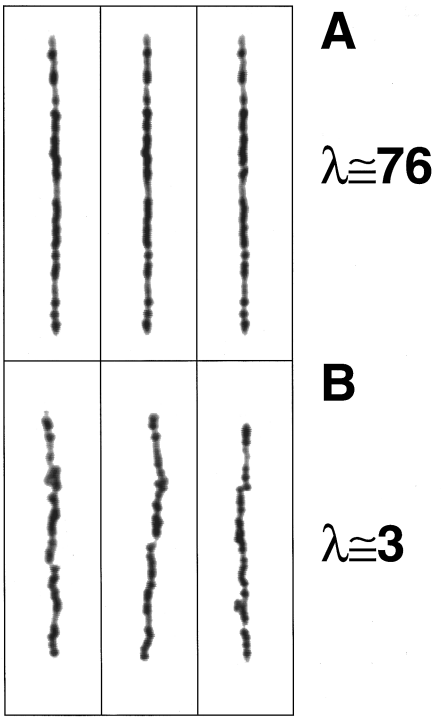

FIG. 1. Video-microscopy snapshots of the thermal fluctuations of a chain comprised of magnetic particles. The magnetic field is applied anisotropically in the chain direction. (a) Chain is ''stiff'' under a strong magnetic field. Dipole-dipole forces dominate. (b) Chain exhibits larger thermal fluctuations under a weak magnetic field.

$$\lambda=\frac{\pi\mu_0\chi^2H_0^2a^3}{9k_BT}. \tag{2}$$

Here, λ describes the ratio between the competing dipole-dipole energy and thermal disordering energy and is obtained by equating the dipole-dipole interaction energy of two particles in contact (1) to k_BT.

$$U(r=2a,\theta=\pi)/k_BT=-\lambda. \tag{3}$$

The denominator in Eq. (2) describes the thermal disordering, where k_B is the Boltzmann constant and T is the absolute temperature. The numerator in Eq. (2) describes the dipole-dipole interaction energy, where μ_0 is the magnetic permeability of the vacuum, χ is the magnetic susceptibility of the paramagnetic particles, H_0 is the applied magnetic field, and a is the particle radius. For a system consisting of two particles, the critical value of λ for which the particles aggregate is exactly $\lambda_c=1$. In a system comprised of many particles, as in a chain, one expects $\lambda_c<1$.

Figure 1 shows two typical series of images of different realizations of a fluctuating magnetic chain when subjected to different magnetic field strengths. When $\lambda=3$, the magnetic particles are connected into a long chain which exhibits thermal fluctuations larger than in the case $\lambda=76$, for which the magnetic chain behaves like a rigid rod.

In contrast to linear-chain formation, the subsequent slow lateral column formation (chain-to-chain aggregation) is only poorly understood [11,12]. Chain aggregation dominates the structural dynamics of MR and ER fluids at long times and, therefore, governs the long time rheology [4]. Chain aggregation into columnar domains also gives rise to the large yield stress and shear-thinning viscosity displayed by both MR and ER fluids [4]. When chain aggregation occurs, elongated domains (or columns) aligned in the field direction are formed. These columnar domains are made of a concentrated solidlike material, which hinders the fluid flow, hence increasing the effective fluid viscosity [4]. The length of the chains formed is governed by the magnetic field strength and concentration of particles.

Halsey and Toor (HT) [11,12] have recently offered an explanation for the long-range interaction between magnetic chains and their subsequent lateral aggregation. These authors describe aggregation by an effective long-range coupling between long wavelength thermal fluctuations of neighboring dipolar chains. If thermal fluctuations are neglected, the transverse magnetic field from the chain decays approximately as $\exp(-r/a)$, where a is the particle radius and r is the distance between the dipolar chain and the observation point. Thus, ''stiff'' chains do not interact strongly if they are separated by a distance greater than their interparticle spacing, a. However, a one-dimensional object such as a dipolar chain imbedded in a three-dimensional space always displays large thermal fluctuations. In this more realistic case, the root mean square of the fluctuating magnetic field normal to the chain decreases as a power law [11]

$$\sqrt{\langle H^2\rangle}\approx\frac{\sqrt{kTa^2}}{r^2}, \tag{4}$$

which should yield a long-range, fluctuation-induced dipolar interaction between chains. The resulting fluctuating field can generate either an attractive or a repulsive interaction between chains. It is remarkable that this fluctuation-mediated magnetic field and the associated interaction are independent of the applied field, H_0. The HT model [11] explains this result by an exact compensation effect between a quadratic decrease of the magnitude of the fluctuations and a corresponding quadratic increase of the dipole-dipole interaction potential with the field strength. Therefore, this fluctuation-induced long-range interaction should exactly compensate the shorter-range dipolar interaction (1) for any field strength. No experiment [3,6] had yet directly supported or rejected the HT model of fluctuation-mediated chain interaction.

B. TIME AND SPACE CORRELATION FUNCTIONS

In order to test the HT model [11] and characterize the thermal fluctuations of a single dipolar chain, one introduces two types of ensemble-averaged correlation functions:

$$C(x,x')\equiv\sqrt{\langle[h(x)-h(x')]^2\rangle}, \tag{5}$$

$$C(x,x',t,t')\equiv\sqrt{\langle[h(x,t)-h(x',t']^2\rangle}. \tag{6}$$

Here, $h(x,t)$ is the local, instantaneous deflection of the probed magnetic chain with respect to an axis placed parallel to the field direction at an arbitrary origin. Figure 2 illustrates how $h(x)$ is defined as the distance from an arbitrary axis oriented parallel to the field direction to a point x of the chain. The $\langle\cdots\rangle$ symbol in Eqs. (5) and (6) defines ensemble averages of independent realizations of a fluctuating chain. Equation (5) determines the static height-height correlation along the chain. This correlation function describes the steady-state, equilibrium spatial ''roughness'' of the one-dimensional solid chain. Equation (6) determines the time-dependent height-height correlation along the chain and describes the relaxation dynamics of the chain. $C(x,x')$ and $C(x,x',t,t')$ describe how fast two points along a chain become decorrelated.

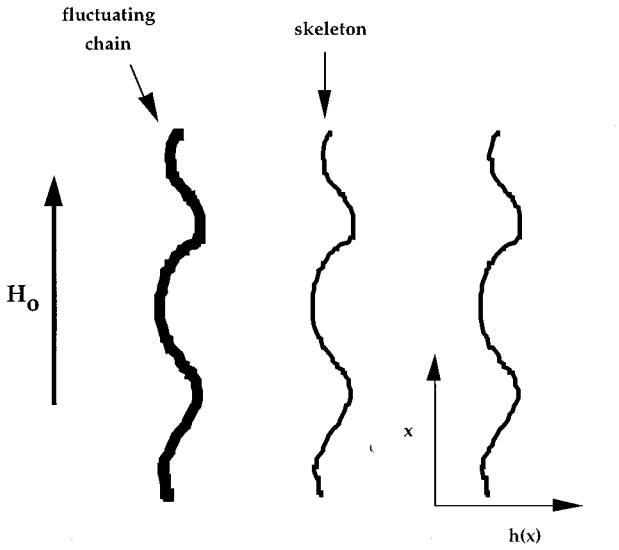

FIG. 2. Schematic of a single-chain image analysis. Image of a chain is binarized and skeletonized. The pixel coordinates of the skeletonized chain are recorded and used to calculate the correlation functions $C(x,x')$ and $C(x,x',t,t')$. Note that $h(x)$ is the horizontal coordinate in this schematic.

The dipolar Hamiltonian describing the chain structure in a magnetic field is time independent; therefore all the associated ensemble averages are invariant under time translation. Similarly, due to the symmetry of the system, the chain structure is invariant under spatial translation. A consequence of this dual space and time invariance is that the static and dynamic correlation functions (5) and (6) do not depend on x, x', t, and t' individually, but on the differences $|x-x'|$ and $|t-t'|$. Hence,

$$C(x,x')=C(|x-x'|)$$

and

$$C(x,x',t,t')=C(|x-x'|,|t-t'|). \tag{7}$$

To study the mechanism of lateral coalescence and test the HT model [11], the static and dynamic fluctuation spectra of a dipolar chain composed of monodisperse particles are measured as a function of the control parameters of the system such as field strength and suspension concentration. Video-microscopy measurements of the chain-fluctuation spectra provide both a direct test of HT theory [11] and a

new insight into the problem of chain aggregation, especially regarding the fluctuation dynamics of dipolar chains.

If we assume that the growth and steady-state fluctuation spectra follow scaling power laws, we can write

$$C(x,t) \approx t^{\beta} \quad \text{for } t \ll t_x \text{ (unsteady state)}, \tag{8}$$

$$C(x,t) \approx x^{\alpha} \quad \text{for } t \gg t_x \text{ (steady state)}, \tag{9}$$

$$t_x \approx x^z. \tag{10}$$

Here, t_x is the crossover time scale which delimitates the initial growth regime of the fluctuations at short times ($t \ll t_x$), from the steady-state regime at long times ($t \gg t_x$). α, β, and z are the roughness exponent, the growth exponent, and the dynamic exponent, respectively: α characterizes the steady-state roughness of the one-dimensional magnetic chain, β characterizes the initial stage of the relaxation of the magnetic chain before the chain reaches a new steady state, and z characterizes how fast the chain reaches this new steady state. According to the HT model [11], $\alpha = \frac{1}{2}$, which can be obtained from the assumption of Gaussian independent fluctuations. In writing Eqs. (8)–(10), the space and time invariance of the chain structure and equilibrium dynamics have been used.

Two key assumptions underlie HT theory [11] and the associated predictive Eq. (4): (1) The static fluctuation spectrum of an individual dipolar chain is that of a directed random walk; (2) hydrodynamic interactions caused by the local motion of the chained particles do not influence the long-range interactions between chains. Using video-microscopy measurements of a single fluctuating magnetic chain and Monte Carlo simulations, we shall test these two assumptions.

III. MATERIALS

Aqueous suspensions of monodisperse paramagnetic particles purchased from Seradyn Inc. are used in this work. The particles are spheres of polystyrene with 40% content of magnetite (Fe_3O_4) encapsulated by copolymerization. These paramagnetic particles have a diameter of $2a = 0.902$ μm, as measured by quasielastic light scattering, and a magnetic susceptibility $\chi = 0.66 \pm 0.09$. The density of the original aqueous suspension (5% w/w solids in purified water) is 1.4 g/cm^3 and the particles are stabilized with surfactant.

IV. MEASUREMENTS OF THE PLANAR SPECTRA OF A SINGLE MAGNETIC CHAIN

We now describe the protocols used in the single-chain dynamics experiments. Using video microscopy, two aspects of chain fluctuation are examined: steady-state equilibrium conformations and dynamic equilibrium conformations, yielding $C(x,x')$, $C(x,x',t,t')$, and t_x. Both studies employ a similar experimental setup, but different image acquisition schemes. A sample of the magnetic suspension of spherical magnetizable particles is introduced into a capillary tube with a rectangular cross section which is then sealed and placed on a microslide. The microslide is placed between two coaxial Helmholtz coils which can generate a homogeneous magnetic field H_0 of up to 54 G. This assembly is placed on a microscope stage (Zeiss Axiovert inverted microscope) and images are captured via a solid-state charge-coupled device video camera (COHU, Inc.) with fixed intensity gain. Image analysis software based on NIH-Image (public-domain software developed at the National Institutes of Health) has been custom designed to process the large quantity of images produced and calculate the fluctuation spectrum profiles, as outlined in Eqs. (5) and (6).

The exponent α, which characterizes the steady-state roughness, is calculated from Eq. (5) using 300 images from independent steady-state conformations of a single, one-particle-thick magnetic chain. The images are acquired with a sufficiently large time elapsed between frames to assure that the chain position recorded in one frame is independent of that in the previous frame. Since it takes 4.6 s for a particle to diffuse its own diameter, an elapsed time about twice the self-diffusion time (about 8 s) was selected. Here, D and $\eta \cong 1$ cP are the self-diffusion constant of one particle suspended in water and the viscosity of the suspending fluid at room temperature. Using the parameters provided previously for a, χ, and H_0 in Eq. (2), one finds that λ has an upper limit of 78. The suspending fluid used is either water or binary solutions of glycerol and water, depending on the desired suspension viscosity. The growth, roughness, and dynamic exponents are calculated from measurements of the spectra $C(x,x')$ and $C(x,x',t,t')$ using Eqs. (5) and (6).

Image processing follows a three-step protocol (Fig. 2). The 256 pixel, gray-scale image of a chain is first binarized (pixels are reduced to either black or white). This image is then skeletonized (converted to a one-pixel-thick chain via a self-consistent ''pruning'' procedure). Finally, the pixel coordinates $(x,h(x,t))$ of points along the chain are obtained. This image processing procedure greatly enhances the spatial resolution of the positions of the spheres that compose a chain. The correlation functions $C(x,x')$ and $C(x,x',t,t')$ are calculated using the length and time invariance properties of the problem. Since the quality of the statistics depends largely on the number of data samples collected, this quality of the statistics decreases rapidly with increasing values of $|x-x'|$. The long length-scale structure of a fluctuating chain is resolved using large collections of images of independent chain configurations.

To measure the fluctuation spectrum of an isolated dipolar chain, video-microscopy experiments using suspensions of low volume fractions $\varphi < 0.08\%$ are conducted. Upon application of a magnetic field on such a dilute suspension, well-separated, one-particle-thick chains are generated and lateral chain interaction is minimized as the interspacing between chains is relatively large (30–60 particle radii).

Chains of between 30 and 120 particles are formed at high magnetic field ($\lambda > \lambda_c$), which is subsequently decreased to allow for the probed chain to fluctuate. Images of a single chain are recorded, analyzed, and the correlation functions are calculated. The formation of chains follows a typical pattern: in the absence of a magnetic field, the suspended particles move about randomly due to thermal forces; upon the application of a strong magnetic field, dipole-dipole forces dominate and particles begin to aggregate forming growing chains; this growth continues until the chains approach a constant length, which is dependent on the particle concentration and magnetic field strength. The chains undulate due

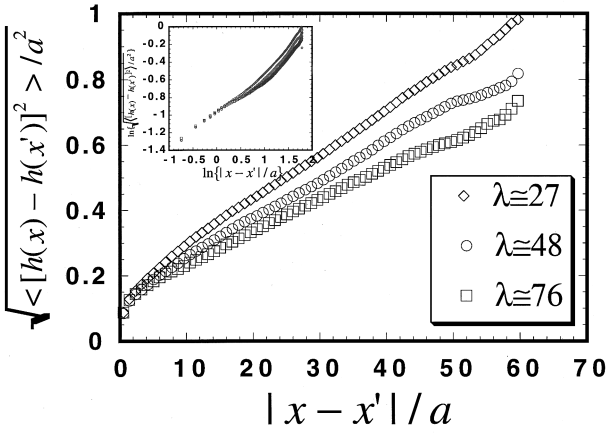

FIG. 3. Steady-state correlation function of a single magnetic chain for three increasing magnetic field strengths. The inset shows the log-log curve of Eq. (5), from which the exponent α can be determined. An average of the three experiments yields $\alpha=0.53\pm0.02$. Only 20% of the data points are shown here.

to random thermal fluctuations with a magnitude decreasing with increasing magnetic field strength.

In order to obtain meaningful statistics, many images of independent realizations of a fluctuating chain need to be captured. The steady-state experiments utilize 300 frames while the dynamic experiments use 500 frames. In order to obtain meaningful statistics, more images are necessary to monitor the roughness dynamics. Our video-microscopy system is limited to the video rate of image capture (20 Hz). It is possible to improve the time resolution in the dynamic experiments by using a more viscous suspending fluid comprised of a glycerol-water mixture. This has the effect of slowing down the chain fluctuations, which results in better image sampling.

V. EXPERIMENTAL RESULTS AND DISCUSSION

The dynamic, growth, and roughness exponents are calculated as a function of field strength using Eqs. (5) and (6). From Fig. 3, we find

$$C(x,x')\approx|x-x'|^{\alpha} \quad \text{with} \quad \alpha=0.53\pm0.02 \quad (|t-t'|\gg t_x), \tag{11}$$

which suggests that the fluctuations grow in a fashion similar to that of a biased random walk: $C(x,x')\approx|x-x'|^{1/2}$. Figure 3 shows the fluctuation growth profile as a function of interspacing distance between particles. Each curve represents an experiment performed at a different magnetic field strength. Notice that, as the magnetic field strength increases (dipole-dipole forces increase), the size of the fluctuations decreases. The limiting case, that of an infinitely strong field, would show no fluctuations or a chain of particles which behaves like a rigid rod. The exponent α was found to be independent of the magnetic field strength.

The studies of the dynamic-equilibrium case yield a value for β which describes the initial growth of chain fluctuations as a function of time. Figure 4 yields

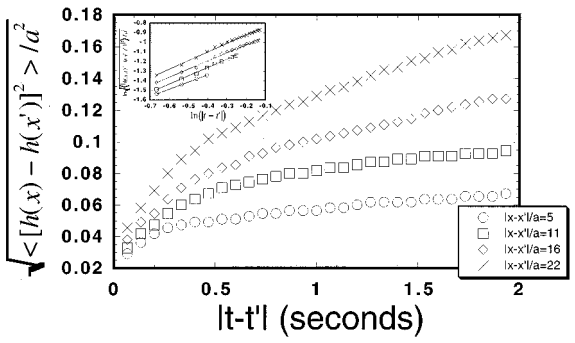

FIG. 4. Dynamic correlation function of a single magnetic chain for three increasing magnetic field strengths. Each curve represents the correlation function for a different $|x-x'|/a$. The inset displays the log-log curve of Eq. (6), from which the exponent β can be determined. An average of the four data sets yields $\beta=0.35\pm0.05<\frac{1}{2}$. Only 20% of the data points are shown here.

$$C(x,x',t,t')\approx|t-t'|^{\beta} \quad \text{with} \quad \beta=0.35\pm0.05 \quad (|t-t'|\ll t_x). \tag{12}$$

In the purely diffusional case, this value would approach that of Brownian diffusion, or $\beta=\frac{1}{2}$. Figure 4 also reveals two distinct phases of growth for the dynamic correlation function. These two phases can be partially explained by analogy with a polymer Rouse chain. The Rouse model of relaxation of a connected polymer chain [31] predicts that the root mean square (rms) displacement of a Rouse chain link grows as $t^{1/4}$ over time intervals smaller than the maximum relaxation time t_x, and only for $t>t_x$ does it become proportional to $t^{1/2}$ as in the ordinary diffusion of a Brownian particle. The results shown in Fig. 4 seem to support this idea, to the extent that the growth exponent is smaller than $\frac{1}{2}$ at times smaller than t_x.

The crossover time t_x increases with $|x-x'|/a$ because larger length scales $|x-x'|/a$ relax more slowly and, hence, take longer to reach a steady-state fluctuation size. To compute t_x, we arbitrarily define a saturation time as the moment at which $C(x,x',t,t')$ reaches 90% of its steady-state value,

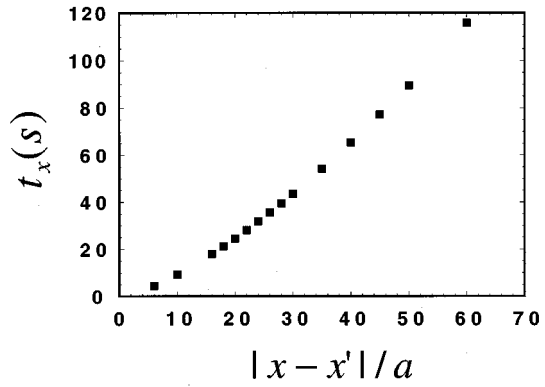

FIG. 5. Crossover time (or saturation time) as a function of $|x-x'|/a$. The linear fit of this curve yields $t_x\approx|x-x'|^z$ with $z=1.41\pm0.18$.

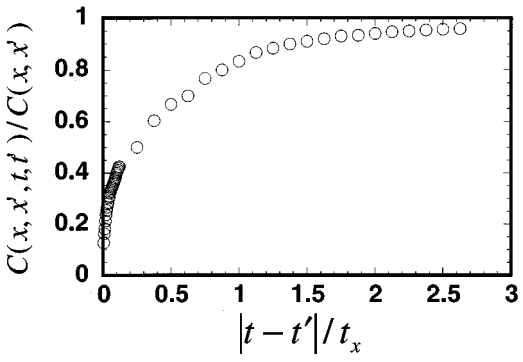

FIG. 6. Scaled correlation function for a single magnetic chain. All data in Figs. 3 and 4 collapse onto a single curve, yielding $z=\alpha/\beta$. Only 5% of the data points are shown here.

$C(x,x')$. Figure 5 displays the crossover time (or saturation time) t_x at which the one-dimensional magnetic line crosses over from the behavior described by Eq. (12) to that described by Eq. (11) as a function of $|x-x'|/a$. A linear fit of the log-log plot of t_x vs $|x-x'|/a$ yields

$$t_x \approx |x-x'|^z \quad \text{with} \quad z=1.41\pm 0.14. \tag{13}$$

We can summarize results (11)–(13) by rescaling the dynamic correlation function $C(x,x',t,t')$ with its saturated value $C(x,x')$ and the time difference $|t-t'|$ by t_x. Figure 6 collapses the data into a single curve. This result suggests that we can write

$$\frac{C(x,x',t,t')}{|x-x'|^{\alpha}} \approx \psi\left(\frac{|t-t'|}{t_x}\right), \tag{14}$$

where ψ is a scaling function of the dimensionless time $|t-t'|/t_x$. We can rewrite this last equation as

$$C(x,x',t,t') \approx |x-x'|^{\alpha}\psi\left(\frac{|t-t'|}{t_x}\right). \tag{15}$$

Of course, $\psi(u)\approx u^{\beta}$ for $u\ll 1$ and $\psi(u)\approx$const for $u\gg 1$. In view of this important result, we can recalculate what the value of the dynamic exponent z should be. At the crossover point,

$$C(x,x',t,t') \equiv C(|x-x'|,|t-t'|) = C(|x-x'|,t_x) \approx t_x^{\beta}.$$

At the same crossover point, $C(|x-x'|,t_x)\approx |x-x'|^{\alpha}$. Therefore, $|x-x'|^{\alpha}\approx t_x^{\beta}$, which according to Eq. (10), implies the following scaling law for the nonindependent exponents α, β, and z:

$$z=\frac{\alpha}{\beta}\cong 1.51, \tag{16}$$

in remarkable agreement with our experimental value (13). Of course, the values of the dynamic exponents z and β that describe the fluctuation dynamics of a single magnetic chain should not necessarily compare with the kinetic exponents that describe the domain growth in concentrated MR or ER suspensions subject to the sudden inception of an electric [3] or a magnetic field [23]. Note that we experimentally verified

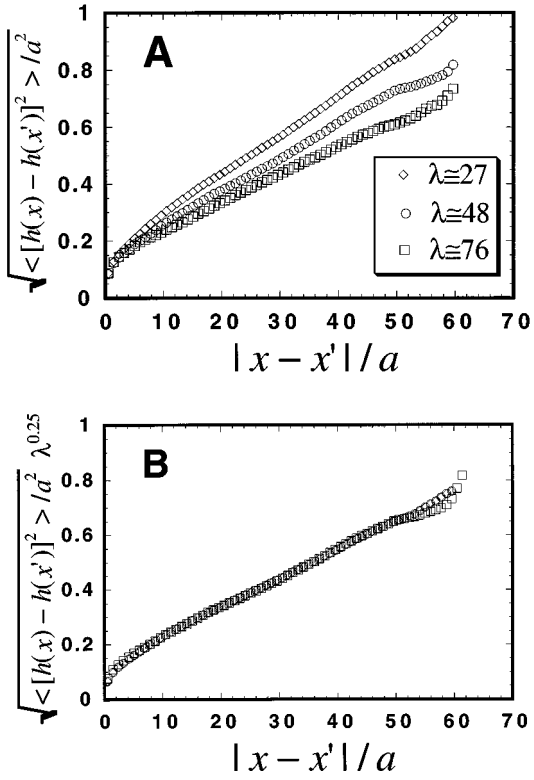

FIG. 7. Collapse of the steady-state correlation functions into a single curve by multiplying $C(x,x')$ by $\lambda^{0.25}$. (a) Steady-state correlation function showing growth of correlation similar to a biased random walk. (b) A good universal curve is obtained after rescaling the correlation functions with $\lambda^{0.25}$. Only 20% of the data points are shown here.

that the growth, roughness, and dynamic exponents are independent of the quiescent viscosity of the suspending fluid.

In order to find the scaling dependence of $C(x,x')$ with respect to λ, we assume the relation

$$C(x,x') \approx \frac{f(|x-x'|)}{\lambda^{\varepsilon}} \quad (|t-t'| \gg t_x), \tag{17}$$

where f is another scaling function of the argument $|x-x'|$. Both sides of Eq. (17) can be multiplied by λ^{ε} and we can collapse the correlation profiles to a ''master'' curve. The value ε which results in a good collapse of the correlation profiles (Fig. 7) is found to be $\varepsilon\cong 0.25$ or

$$C(x,x') \approx \lambda^{-\varepsilon} \quad \text{with} \quad \varepsilon=0.25\pm 0.02. \tag{18}$$

Figures 7(a) and 7(b) display the correlation curves before and after scaling of the correlation function by $\lambda^{0.25}$. As discussed next, this result has important implications.

According to the HT model [11], long-range chain interaction is controlled by two factors: (1) dipole-dipole interactions and (2) the long-range fluctuation-mediated transverse magnetic field. On the one hand, the amplitude of the thermal fluctuations is decreased as the applied magnetic field is increased. By symmetry, the HT model [11] predicts that $C(x,x')\sim 1/\lambda$. On the other hand, the amplitude of the dipole-dipole interaction potential increases as $U(r,\theta)\sim\lambda$. Therefore, according to the HT model [11], this long-range

interaction between chains is independent of the applied field with the magnitude of interaction $\sim C(x,x')U(r,\theta) \sim \lambda/\lambda = 1$. In contrast with the model, the experimental results imply that the dependence of these two interactions with λ does not exactly compensate and that the controlling factor is the applied magnetic field. Our experimental results suggest that the efficiency of the long-range chain interactions scales as $\lambda/\lambda^{0.25} = \lambda^{0.75}$.

To verify this assertion, we generated long magnetic chains following the usual protocol described earlier, and we either reduced or increased the field strength by changing the applied electric current. In most cases (more than 90% of all experiments), we found that increasing the field strength and, therefore increasing the dipole-dipole interaction potential, was indeed more efficient in bringing initially isolated chains together than decreasing the field strength, and therefore increasing the size of thermal fluctuations. One possible explanation for the discrepancy between the predictions of the HT model and our experimental observations might simply be due to the fact that this model assumed infinitely long dipolar chains. This model applies for ER fluids for which the chains span the gap between the conducting electrodes, which generate images dipoles. The resulting dipolar chains are effectively infinite. In the case of MR fluids, the chains are not infinite and the resulting finite chains act as interacting dipoles at large length scales. Further theoretical work needs to be done to understand the origin of the unexpected exponent, $C(x,x') \approx \lambda^{-\varepsilon}$ with $\varepsilon = 0.25 \pm 0.02$. By symmetry, we would expect $C(x,x') \approx \lambda^{-1}$. This might imply that there must be another energy scale entering the local interactions. Below, we verify that this energy scale is not set by hydrodynamic interactions.

VI. MONTE CARLO SIMULATIONS

A. Introduction

As discussed previously, chain formation in dipolar fluids and the subsequent chain aggregation are caused by the magnetic interparticle interactions, which are responsible for the unusual viscoelastic properties and the stability of the magnetic fluid. One way of probing these interparticle interactions is through the use of molecular simulations. In this work, we use Monte Carlo simulations to probe the spectrum of chain fluctuation and allow for direct comparison with the video-microscopy measurements.

The fundamental basis for the application of Monte Carlo (MC) simulations to magnetic fluids has already been presented in detail by Chantrell *et al.* [32] and Menear, Bradbury, and Chantrell [33]. As in their simulations, our system consists of a colloidal suspension of magnetizable particles, which display only very small van der Waals forces. The dipole-dipole energy of the particles is given by Eq. (1), where θ is the angle between the direction of the magnetic field and the line of centers of the two particles and we ignore higher order dipolar moments.

The Monte Carlo method used here is based on that proposed by Metropolis in 1953 (Allen and Tildesley [34]). We calculate the energy $E(i)$ of the system of N particles with coordinate vector $\mathbf{x}(i)$. The particles are then moved at random to new coordinates $\mathbf{x}'(i)$ and the new energy $E'(i)$ is also calculated. Here, the index i represents the number of the MC step and, during each move, the particles are restricted to move within a sphere of size $6a$.

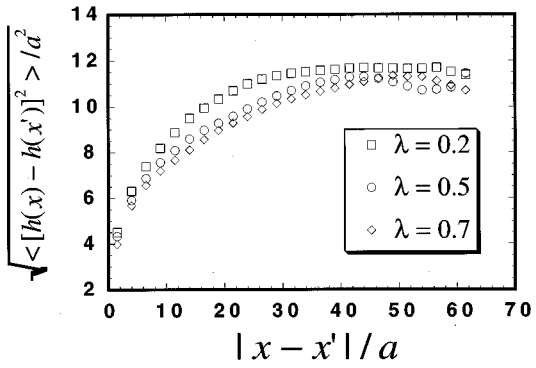

FIG. 8. Steady-state correlation function for a single chain obtained by Monte Carlo simulations. This simulation used 64 particles and 400 configurations. Each curve represents a simulation performed at a different magnetic field strength. Only 20% of the data points are shown here.

If the energy difference $\Delta E = E'(i) - E(i)$ is negative, the move is accepted and the particles keep their new coordinates. If, instead, ΔE is positive, a random number X ($0 < X < 1$) is generated and compared to $\exp(-\Delta E/k_B T)$. If $\exp(-\Delta E/k_B T) > X$, the move is accepted. However, if $X > \exp(-\Delta E/k_B T)$, the move is rejected and the particles are returned to their original position. This procedure is repeated for all the N particles of a chain at each step and, after a sufficiently large number of moves, the resulting conformation represents a good picture of the system in equilibrium. Periodic boundary conditions are used here.

Our simulation scheme differs from previous works [32,33] in that the initial state corresponds to a set of N particles connected to each other in a rigid-rod-like configuration and are subsequently subjected to a magnetic field of desired strength, which allows the chain to relax and fluctuate. Previous works [32,33] focused on the kinetics of chain formation for which the appropriate initial state is a random configuration of the set of N particles. We simulate the thermal fluctuations of a single chain of variable length ($N = 32$ particles to $N = 108$ particles), where all particles of the chain are moved in each MC step; the motion of one particle at a time is not sufficient to generate independent configurations and therefore calculate the ensemble averages. The dimensionless parameter λ (which is the ratio between the induced dipole-dipole interactions and the thermal energy) and the number of particles in the chain are the only parameters in the MC simulation. The fluctuation spectra of the chains were simulated using different magnetic field strengths and chain lengths. The configurations generated by the MC simulations were studied by calculating the same correlation functions that were used to treat the experimental data [Eqs. (5) and (6)]. The results are presented in Figs. 8–11.

B. Results

In Fig. 8, we present the correlation function for a chain of 64 particles, subjected to three different field strengths, given by $\lambda = 0.2$, 0.5, and 0.7. As can be seen from the plot, the behavior observed is qualitatively the same as observed from the experiments. From the log-log curves of $C(x,x')$ vs

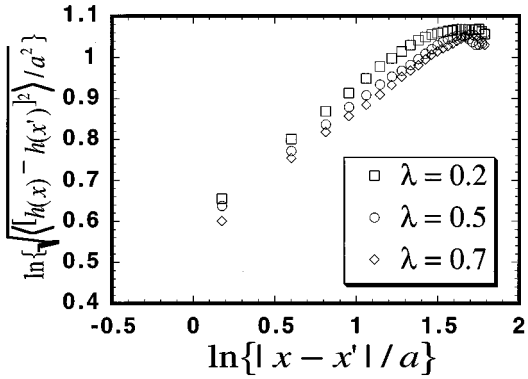

FIG. 9. Log-log curve of Eq. (5) for the simulation of 64 particles. The roughness exponent is found to be $\alpha=0.31\pm0.03$. Only 20% of the data points are shown here.

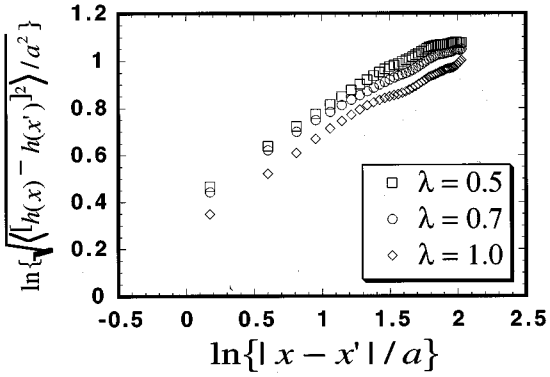

FIG. 11. Log-log curve of Eq. (5) for the simulation of 108 particles. The roughness exponent is found to be $\alpha=0.39\pm0.02$. Only 20% of the data points are shown here.

$|x-x'|/a$ (see Fig. 9), we obtain the roughness exponent $\alpha=0.39\pm0.03$. Figure 10 presents the same analysis for a chain of 108 particles and subjected to magnetic field strengths given by $\lambda=0.5$, 0.7, and 1. The behavior again is qualitatively the same as seen before and this time the exponent obtained from Fig. 11 is $\alpha=0.44\pm0.02$. Effects of the length of the chain can be noticed from the previous results: when the size of the chain in the simulation is increased, the ''roughness'' exponent increases, approaching the value found in the experiments.

We observe a saturation effect of the correlation function for large length scales. The onset of this saturation can be viewed as the distance after which there is no effect of the fluctuations of the particles on each other. In all cases presented here, the number of configurations used to calculate the ensemble averages was 400 and the total number of MC steps during the simulations were of the order 10^6, which is required to ensure that the configurations used for the averaging are independent from each other. Steady-state height-height correlation functions $C(x,x')$ were calculated as a function of λ and rescaled (not shown here) as $C(x,x')/\lambda^{\varepsilon}$. The collapse of the curves onto a single scaling curve is obtained for $\varepsilon=0.27\pm0.02$, in agreement with our video-microscopy measurements. Since these Monte Carlo simulations ignore hydrodynamic interactions, hydrodynamic interactions do not set a new energy scale, which could explain the unexpected exponent ε.

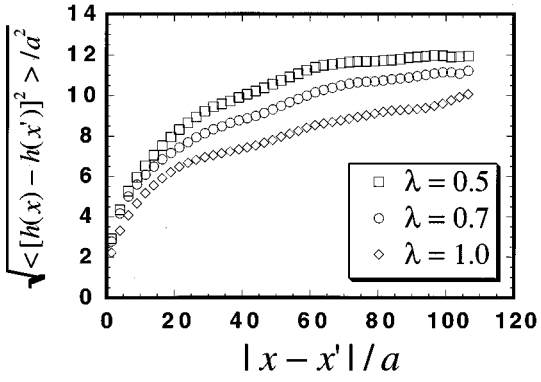

FIG. 10. Steady-state correlation function for a single chain from the Monte Carlo simulations. This simulation used 108 particles and 400 configurations. Each curve represents a simulation performed at a different magnetic field strength. Only 20% of the data points are shown here.

We also probe the aggregation of chains by simulating the behavior of two chains that are initially far apart. The same procedure described previously is used in this case but, even after a sufficiently large number of steps, the two chains are still away from each other and we are not able to reproduce the experimental observations. The fact that the dipole-dipole interactions alone cannot account for the chain aggregation leads us to believe that long-range hydrodynamic effects are important and should be taken into account when simulating the chain aggregation. Molecular dynamics studies of the fluctuation dynamics of magnetic chains are underway and these simulations will include hydrodynamic effects.

VII. CONCLUSIONS

''Tunable'' fluids have generated acute interest due to the possibility of their use in fast-response mechanical devices. This paper presented video-microscopy observations and MC simulations, which characterized the steady-state and relaxation spectra of a single magnetic chain. This study shows that steady-state, single-chain fluctuations behave in a fashion similar to that of a biased random walk with respect to interspacing distance along the chain, $C(x,x')\approx|x-x'|^{\alpha}$ with $\alpha=0.53\pm0.02$. The numerical results agree qualitatively and semiquantitatively with the experimental results for the single-chain steady-state fluctuations. The studies of the dynamic fluctuation show that single-chain time-dependent fluctuations grow slower than diffusion due to the fact that the particles are part of a connected object and this connectivity reduces the freedom of movement. The initial growth of the chain roughening (or relaxation at early times) is characterized by a growth exponent β such that $C(x,x',t,t')\approx|t-t'|^{\beta}$ with $\beta=0.35\pm0.05$. All data can be collapsed onto a single curve according to $C(x,x',t,t')\approx|x-x'|^{\alpha}\psi(|t-t'|/|x-x'|^{z})$ with $\alpha\cong0.53$, $z\cong1.41$, and $\beta=\alpha/z\cong0.35$.

Our experimental results also indicate that long-range fluctuation-mediated interaction and the shorter-range dipole-dipole interaction are not in true compensation: the

applied magnetic field is the dominating factor in the mechanism of chain interaction.

ACKNOWLEDGMENTS

The authors thank M. O. Robbins, S. Roux, and M. Fermigier for fruitful discussions and acknowledge the National Science Foundation (Grant No. CTS9502810) and donors of The Petroleum Research Foundation administered by the American Chemical Society (Grant No. ACSPRF29779G9) for financial support. A. S. Silva acknowledges the National Research Council of Brazil–CNPq/BR (Grant No. 200731/93-9) for financial support.

[1] Economist **328**, 77 (1993); **328**, 90 (1993).
[2] J. D. Carlson and K. D. Weiss, Machine Design **61-64** (1994).
[3] T. C. Halsey, Science **258**, 761 (1992).
[4] T. C. Halsey, J. E. Martin, and D. Adolf, Phys. Rev. Lett. **68**, 1519 (1992).
[5] W. M. Winslow, J. Appl. Phys. **20**, 1137 (1949).
[6] D. L. Klass and T. W. Martinek, J. Appl. Phys. **38**, 67 (1967).
[7] D. L. Klass and T. W. Martinek, J. Appl. Phys. **38**, 75 (1967).
[8] A. P. Gast and C. F. Zukowski, Adv. Colloids Interface Sci. **30**, 153 (1989).
[9] Polyscience Inc., Annual Report, 1995 (unpublished).
[10] D. Wirtz, Phys. Rev. Lett. **75**, 2436 (1995).
[11] T. C. Halsey and W. Toor, J. Stat. Phys. **61**, 1257 (1990).
[12] T. C. Halsey and W. Toor, Phys. Rev. Lett. **65**, 2820 (1990).
[13] H. Block and J. P. Kelly, J. Phys. D. Appl. Phys. **21**, 1661 (1988).
[14] D. Scott and J. Yamaguchi, Autom. Eng. **93**, 75 (1985).
[15] F. E. Filisko and W. H. Armstrong, U.S. Patent No. 4,744, 914 (1988).
[16] K. Sano and M. Doi, J. Phys. Soc. Jpn. **52**, 2810 (1983).
[17] H. See and M. Doi, J. Phys. Soc. Jpn. **60**, 2778 (1991).
[18] J. T. Woestman and A. Widom, Phys. Rev. E **48**, 1995 (1993).
[19] P. C. Jordon, Mol. Phys. **25**, 961 (1973).
[20] A. T. Skjeltorp, J. Appl. Phys. **57**, 3285 (1985).
[21] A. T. Skjeltorp, in *Complex Fluids*, edited by L. Garrido (Springer-Verlag, Heidelberg, 1992), p. 243.
[22] J.-Cl. Bacri and R. Perzynski, in *Complex Fluids* (Ref. [21]), pp. 85, 99.
[23] M. Fermigier and A. P. Gast, J. Colloids Interface Sci. **154**, 522 (1992).
[24] Z. Mimouni, G. Bossis, C. Mathis, A. Meunier, and C. Paparoditis, Prog. Colloid Polym. Sci. **81**, 120 (1990).
[25] E. Lemaire and G. Bossis, J. Phys. D **24**, 1473 (1991).
[26] Y. Grasselli, G. Bossis, and E. Lemaire, J. Phys. (France) II **4**, 253 (1994).
[27] D. Wirtz and M. Fermigier, Phys. Rev. Lett. **72**, 2294 (1994).
[28] D. Wirtz and M. Fermigier, Langmuir **11**, 398 (1995).
[29] M. J. Stevens and G. S. Grest, Phys. Rev. Lett. **72**, 3686 (1994).
[30] J. E. Stangroom, Phys. Technol. **14**, 290 (1983).
[31] A. Y. Grosberg and A. R. Khokhlov, *Statistical Physics of Macromolecules* (AIP Press, New York, 1994).
[32] R. W. Chantrell, A. Bradbury, J. Popplewell and S. W. Charles, J. Phys. D **13**, L119 (1980).
[33] S. Menear, A. Bradbury, and R. W. Chantrell, J. Magn. Magn. Mater. **43**, 166 (1984).
[34] M. P. Allen and D. J. Tildesley, *Computer Simulation of Liquids* (Oxford Science, New York, 1989).